Exploration of the Pharmacophore of 3-Alkyl-5-Arylimidazolidinediones as New CB$_1$ Cannabinoid Receptor Ligands and Potential Antagonists: Synthesis, Lipophilicity, Affinity, and Molecular Modeling

Frédéric Ooms,[†] Johan Wouters,[‡,||] Olivier Oscari,[§] Thierry Happaerts,[§] Géraldine Bouchard,[†] Pierre-Alain Carrupt,[†] Bernard Testa,[†] and Didier M. Lambert*,[§]

Institut de Chimie Thérapeutique, Ecole de Pharmacie, Université de Lausanne, CH-1015 Lausanne, Switzerland, Laboratoire de Chimie Moléculaire Structurale, Faculté des Sciences, Facultés universitaires Notre Dame de la Paix, Rue de Bruxelles 61, B-5000 Namur, Belgium, and Unité de Chimie pharmaceutique et de Radiopharmacie, Ecole de Pharmacie, Faculté de Médecine, Université catholique de Louvain, Avenue E. Mounier 73 UCL-CMFA 7340, B-1200 Bruxelles, Belgium

A set of 29 3-alkyl 5-arylimidazolidinediones (hydantoins) with affinity for the human cannabinoid CB$_1$ receptor was studied for their lipophilicity and conformational properties in order to delineate a pharmacophore. These molecules constitute a new template for cannabinoid receptor recognition, since (a) their structure differs from that of classical cannabinoid ligands and (b) antagonism is the mechanism of action of at least three compounds (**20**, **21**, and **23**). Indeed, in the [^{35}S]-GTPγS binding assay using rat cerebellum homogenates, they behave as antagonists without any inverse agonism component. Using a set of selected compounds, experimental lipophilicity was measured by RP-HPLC and calculated by a fragmental method (CLOGP) and a conformation-dependent method (CLIP based on the molecular lipophilicity potential). These approaches revealed two models which differentiate the binding mode of nonpolar and polar hydantoins and which could explain, at least for compounds **20**, **21**, and **23**, the mechanism of action of this new family of cannabinoid ligands.

Introduction

Hashish and marijuana, two preparations derived from the Indian hemp *Cannabis sativa L.*, have been used since an unknown number of centuries for their medicinal and psychoactive properties. Δ^9-Tetrahydrocannabinol (THC), the natural product isolated from the plant,[1] is its major psychoactive component. Cannabinoids, by definition, are compounds sharing a common structure with THC; this class includes C$_{21}$ compounds originally isolated from *Cannabis sativa L.* as well as their carboxylic acid derivatives, various analogues, and transformation products. In vivo, THC is readily oxidized to the more potent 11-OH-Δ^9-THC. Chemical modifications of this structure have led to 9-nor-9β-OH-hexahydrocannabinol (HCC), a compound exhibiting enhanced analgesic activity. Pharmacomodulation of THC and HHC gave bicyclic analogues,[2] e.g., CP-47,-497 and CP-55,940. The latter compound in tritiated form became the first suitable radioligand for the cannabinoid (CB) receptors.[3]

To date, two distinct cannabinoid receptors, CB$_1$ and the CB$_2$, have been cloned. The CB$_1$ cannabinoid receptor,[4,5] which was first evidenced by autoradiography and radioligand binding studies using [^{3}H]-CP-55,940, was cloned from the human, rat, and mouse. It is expressed in the brain and some peripheral tissues including testis, ileum, urinary bladder, and vas deferens. An alternative spliced form of the CB$_1$ cannabinoid receptor, named CB$_{1A}$, has also been described, but so far has revealed no peculiar property in terms of ligand recognition and receptor activation.[6] The CB$_2$ cannabinoid receptor was discovered by sequence homology.[7] It is predominantly found in the immune system (spleen, tonsils, immune cells) and was cloned from the same animal species.[7−9] The amino acid sequence of both cannabinoid receptors shows the common characteristics of G-protein coupled receptors, including a lipophilic 7-transmembrane α-helix structure. The transduction mechanisms of cannabinoid receptors involve inhibition of cAMP production through inhibition of adenylate cyclase,[10] inhibition of calcium influx,[11,12] activation of potassium channels,[13] and activation of the MAP kinase pathway.[14] Both types of cannabinoid receptors are sensitive to pertussis toxin, suggesting their predominant coupling to G$_i$-type proteins (G$_i$ and G$_o$ subtypes).

Endogenous ligands (called endocannabinoids) have been discovered. These are long-chain polyunsaturated fatty acids whose carboxylate group is amidated by ethanolamine or esterified by glycerol.[15] The major representatives are anandamide or arachidonoylethanolamide and 2-arachidonoylglycerol. The discovery of endogenous ligands prompted further studies to elucidate the structural requisites and pharmacological properties of CB$_1$ and CB$_2$ receptors. These studies revealed that, in addition to classical cannabinoids, other structurally quite different compounds are CB receptor ligands. The term "cannabinoids" is now applied to any compound with good affinity for the cannabinoid receptors. Cannabinoid ligands are cur-

* To whom correspondence should be addressed. Phone: +32 2 764 7347. Fax: +32 2 764 73 63. E-mail: lambert@cmfa.ucl.ac.be.
† Université de Lausanne.
‡ Facultés universitaires Notre Dame de la Paix.
§ Université catholique de Louvain.
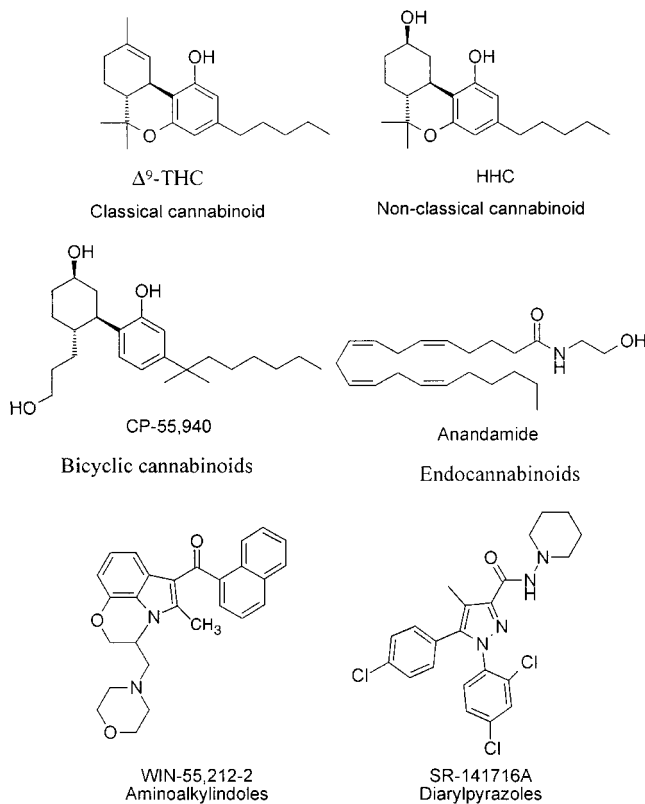|| Present address: Institut de Recherches Microbiologiques Wiame, Av E. Gryson 1, B-1070 Brussels, Belgium.

Figure 1. Representative ligands of the cannabinoid receptors.

Table 1. Structures, Affinity to CB_1 Cannabinoids Receptors, and Lipophilicity of 3-Alkyl-5,5'-diphenylimidazolidinediones **1–24**

compd	R_1	n	R_2	% of displacement at 10 μM^a	lipophilicity^b
1	H	2	$-N(CH_2CH_2)_2O$	<5	2.16
2	H	2	$-N(CH_2)_5$	<15	3.83
3	H	2	$-N(CH_3)_2$	<5	2.83
4	H	2	$-CH_3$	<20	3.84
5	H	3	$-CH_3$	25.1 ± 2.2	4.26
6	H	4	$-CH_3$	35.4 ± 2.9	4.80
7	H	5	$-CH_3$	35.6 ± 1.5	5.37
8	H	7	$-CH_3$	61.2 ± 4.7	6.50
9	H	1	$-C_6H_5$	40.6 ± 3.9	4.11
10	H	0	$-CH(CH_3)_2$	<5	2.89
11	CH_3	2	$-N(CH_2CH_2)_2O$	23.9 ± 1.9	3.49
12	CH_3	5	$-CH_3$	46.8 ± 3.9	6.48
13	CH_3	6	$-CH_3$	51.3 ± 3.8	7.04
14	OCH_3	2	$-N(CH_2CH_2)_2O$	21.7 ± 1.7	2.73
15	OCH_3	5	$-CH_3$	66.6 ± 5.3	5.81
16	F	2	$-N(CH_2CH_2)_2O$	30.3 ± 2.1	2.81
17	F	5	$-CH_3$	40.6 ± 3.1	5.81
18	F	6	$-CH_3$	51.4 ± 2.9	6.42
19	F	7	$-CH_3$	62.5 ± 5.7	6.94
20	Br	2	$-N(CH_2CH_2)_2O$	91.2 ± 7.3	3.86
21	Br	3	$-OH$	88.4 ± 6.7	3.76
22	Br	5	$-CH_3$	72.1 ± 5.3	6.87
23	Br	6	$-CH_3$	89.2 ± 7.6	7.45
24	Br	7	$-CH_3$	80.0 ± 6.0	7.99

^{a} Results are expressed as the percentages of the displaced specific binding of [^{3}H]SR-141716A (mean ± SEM, $n = 3$–5). ^{b} Lipophilicity was calculated using the CLIP method.

Table 2. Structures, Affinity to CB_1 Cannabinoids Receptors, and Lipophilicity of Other (±)-3-Alkyl-5-arylimidazolidinediones **25–29**


compd	n	R	% of displacement at 10 μM^a	lipophilicity^b
25	3	$-CH_3$	<5	2.21
26	5	$-CH_3$	28.8 ± 2.3	3.21
27	2	$-C_6H_5$	64.0 ± 5.6	2.31
28	3	$-C_6H_5$	44.3 ± 3.8	2.80
29	1	naphthyl	59.8 ± 5.1	2.92

^{a,b} See Table 1.

rently classified into at least six groups (Figure 1), namely classical (e.g., Δ^9-THC) and nonclassical cannabinoids (e.g., HHC), bicyclic cannabinoids (e.g., CP-55,940), aminoalkylindoles (e.g., WIN-55,212-2), endocannabinoid analogues (anandamide and 2-arachidonoylglycerol), and diarylpyrazoles (e.g., SR-141716A and SR-144528).

Based on the structure of 1-alkyl-3-(1-naphthoyl)-pyroles and diarylpyrazoles antagonists, 24 3-alkyl-(5,5'-diphenyl)imidazolidinediones were recently synthesized and evaluated as new CB_1 cannabinoid receptor ligands.[16] Five further compounds were prepared and assayed in this work. These 3-alkyl-5-arylhydantoins could constitute a novel template for CB_1 recognition and possibly CB_1 antagonism. They are examined here for structure–affinity relationships using the following approaches:

1. Binding studies to human CB_1 obtained from human CB_1 transfected CHO cells membranes.[16]

2. Preliminary functional test for compounds exhibiting the best affinity (compounds **20**, **21**, and **23**). The functional assay used was the [^{35}S]-GTPγS binding assay in rat cerebellum homogenates.

3. Lipophilicity determination by RP-HPLC of compounds within the complete series of 29 ligands, conversion into log P values as explained below, and comparison with calculated parameters (CLOGP, CLIP).[17–18]

4. Selection of the best lipophilicity predictor and its application to the complete series of 29 hydantoins.

5. Search for qualitative relationships between lipophilicity and affinity.

6. Finally, these derivatives were compared with HHC with a view to obtain a better understanding of the stereoelectronic requisites of binding to the CB_1 cannabinoid receptor. To address this issue, X-ray analysis,

molecular modeling, and molecular field superposition methods were used.

Results and Discussion

Chemistry. The structures of the compounds used in this study are presented in Tables 1 and 2. Synthesis of compounds **1–24** (Table 1) has been described elsewhere.[16] Briefly, 5,5'-diphenylhydantoin was first obtained by the Biltz reaction from benzile, urea, and KOH in ethanol. 5,5'-Diphenylhydantoin was then alkyl-

Scheme 1[a]
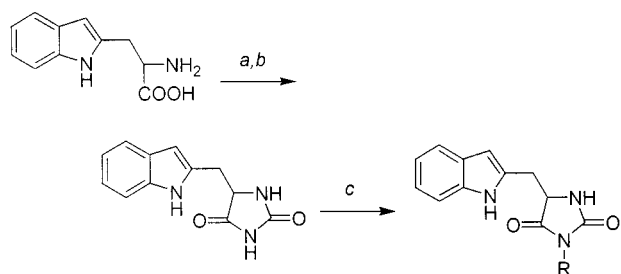
[a] Reagents: (a) KCNO, water, 80 °C, 30 min; (b) HCl, ethanol, reflux 2 h; (c) RCl, K_2CO_3, DMF, room temperature overnight.

Scheme 2[a]
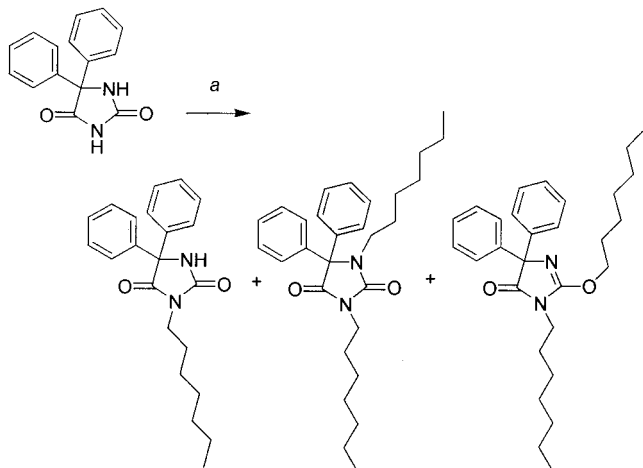
[a] Reagents: (a) chloroheptane, K_2CO_3, DMF.

ated in position N_3 using the respective alkylating agent in K_2CO_3/dimethylformamide. The new analogues **25–29** differing in the 5-substituents were obtained after adaptation of the previously described procedure,[16] as outlined in Scheme 1. Although these reactions are rather straightforward, their success depends on a good temperature control and a correct proportion of alkylating agent. For example, the alkylation of 5,5′-diphenylhydantoin by 1-chloroheptane with potassium carbonate gave an N_1,N_3-dialkyl and an N_3,O-dialkyl product in addition to the desired mono-N_3-alkyl product (Scheme 2). Selectivity in the alkylating step is obtained at low temperature, which may explain the somewhat low yields observed. Moreover, the tryptophan analogues **25–29** have a center of chirality (Table 2) and were not obtained in enantiopure form. The first synthetic step, i.e., the formation of the indolylmethyl-hydantoins, retained the absolute configuration of the starting amino acid, i.e., D- or L-tryptophan. However, the subsequent alkylating process gave a racemate ([α] = 0), and compounds **25–29** were tested as racemates.

Pharmacology. Compounds **1–29** were screened at 10 μM in competitive binding displacement experiments with [^{3}H]-SR-141716A, a selective CB_1 cannabinoid radioligand, in a preparation of transfected CHO membranes expressing the human CB_1 cannabinoid receptor. The results (Tables 1 and 2) are expressed as a percentage of displacement of the specific binding of [^{3}H]-SR-141716A. The most active compounds were then compared to reference cannabinoids (HU-210, CP-55,940, SR-141716A, and WIN-55,212-2) in dose-displacement curves. Under our conditions, saturation experiments

Table 3. K_i Values of Compounds **20**, **21**, and **23** and Reference Cannabinoid Ligands for Human Cannabinoid CB_1 Receptors

compd	K_i (nM) against [^{3}H]SR-141716A
20	70.3 ± 4.3
21	103.2 ± 6.8
23	97.9 ± 5.5
HU210	0.82 ± 0.04
CP 55940	5.2 ± 0.3[a]
SR-141716A	8.9 ± 0.4[a]

gave a K_d of 1.24 ± 0.1 nM and a B_{max} of 47.9 ± 4.7 pmol/mg protein. The K_i of the most active compounds are presented in Table 3. Compounds **20**, **21**, and **23** exhibited interesting K_i values below 100 nM. Neither the addition of 50 μM 5′-guanylylimidodiphosphate (GppNHP),[16] a stable analogue of GTP, nor the use of [^{3}H]-CP-55,940 as radioligand (data not shown) significantly affected the affinity of compounds **20**, **21**, and **23** for the human CB_1 cannabinoid receptor. Taken together, these data suggest that the cannabinoid hydantoins, at least compounds **20**, **21**, and **23**, do not act as agonists for the cannabinoid receptor. Indeed, it is known that agonists of G-protein coupled receptors are sensitive to the addition of stable analogue of GTP.[19] In addition, Kearn and co-workers[20] have shown that [^{3}H]-SR 141716A labels both the active and inactive CB_1 cannabinoid receptors, in contrast to the agonist radioligand, [^{3}H]-CP-55,940, suggesting the use of the latter may reveal higher affinity in the case of agonists. The commercially available radiolabeled guanosine 5′-O-(γ-[^{35}S]thio)triphosphate [^{35}S]-GTPγS was used in a derived binding technique to further characterize the activity of compounds **20**, **21**, and **23** as widely used for cannabinoid receptors (for a review, see ref 21). This assay constitutes a functional measure of the interaction of the receptor and the G-protein, the first step in activation of the G-protein coupled receptors. In addition, whatever the transduction mechanism, it is possible to define the functional activity of a ligand as agonist (positive intrinsic activity), partial agonist (partial positive intrinsic activity), antagonist (no intrinsic activity), or inverse agonist (negative intrinsic activity). In rat cerebellum homogenates which present a high density of CB_1 cannabinoid receptors, HU210 stimulates the [^{35}S]-GTPγS binding with an E_{max} of 267 ± 10% (full agonist) and an EC_{50} of 3.0 (1.2–7.8) nM, whereas SR-141716A shows inverse agonist property as it decreases nucleotide binding by 30.5 ± 2.1% (Figure 2A). Compounds **20**, **21**, and **23** were without intrinsic effect but competitively inhibit HU 210-induced [^{35}S]-GTPγS binding in rat cerebellum homogenates (pK_B values of 6.11 ± 0.14, 6.25 ± 0.06, and 5.74 ± 0.09, respectively) (Figure 2B).

Lipophilicity. The RP-HPLC method was first calibrated with reference compounds of well-known log P values ranging from 0.64 to 3.30 (benzamide, benzyl alcohol, acetanilide, benzaldehyde, phenol, nitrobenzene, benzene, toluene, chlorobenzene, bromobenzene, benzophenone, and naphthalene).[22] The RP-HPLC log k_w indices were correlated with the corresponding log
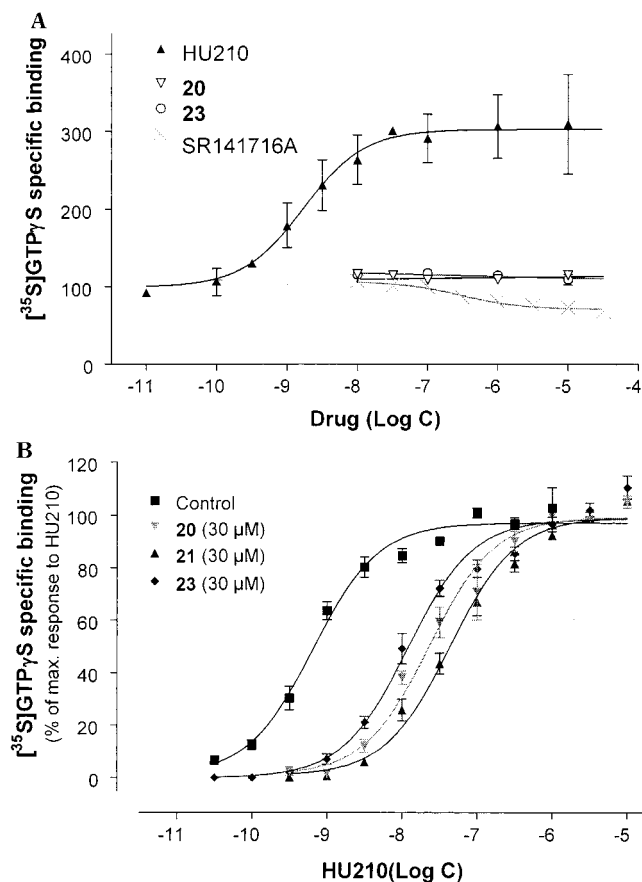
Figure 2. Comparative effects of cannabinoids and compounds **20**, **21**, and **23** on the stimulation [^{35}S]-GTPγS binding in rat cerebellum homogenates. (A) Effects of HU-210 (▲) (full agonist), SR141716A (×) (inverse agonist), **20** (▽), and **23** (○) (full antagonists) on [^{35}S]-GTPγS binding. Data are the mean from at least three separate experiments; vertical lines show SEM. (B) Determination of pK_B values of **20**, **21**, and **23** against HU 210-induced [^{35}S]-GTPγS binding in rat cerebellum membranes. The HU 210 stimulation (from 10^{-5} to $10^{-10.5}$ M) curve is presented in the absence (■) or presence of compounds **20** (▼), **21** (▲), and **23** (◆) (30 μM). Data are the mean from at least three separate experiments; vertical lines show SEM.

P values, yielding the following linear relation:

$$\log P = 1.31(\pm 0.13)\log k_w - 0.362(\pm 0.25)$$

$$(r^2 = 0.92, n = 12, s = 0.28, F = 107.1)$$

This regression equation was used to transform the measured capacity factors (log k_w) of a set of 11 hydantoins (Table 4) into log *P* values. Two computational methods (CLOGP[17] and CLIP[18]) were then applied to predict the lipophilicity of this set of hydantoins. The resulting log *P* values were compared to the experimental values (Table 4). CLOGP yielded a good correlation ($n = 11$, $r^2 = 0.82$, $s = 0.78$, $F = 38.49$), but a better correlation was obtained with CLIP ($n = 11$, $r^2 = 0.89$, $s = 0.58$, $F = 72.35$). This method was thus applied to the complete set of hydantoins, and the log *P* values so calculated were examined for relationships with the CB$_1$ receptor affinity data (Tables 1 and 2).

Structure−Affinity Relationships. The results reported in Table 1 show that affinity for the CB$_1$ receptor increases with the introduction of a para substituent on the phenyl rings. The dibromo deriva-

Table 4. Determination of the Lipophilicity of 12 Representative Compounds: Comparison between Experimental Measurements and Calculations

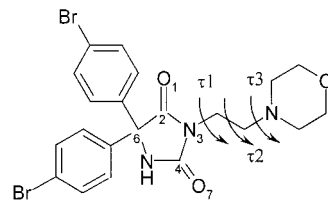| compd	log K_w	log P_{corr}	CLIP[a]	CLOGP[b]
2	4.11	5.02	3.83	2.94
3	3.00	2.94	2.83	1.58
4	2.93	2.86	3.84	3.31
5	3.46	3.44	4.26	3.84
7	4.32	4.39	5.37	4.90
20	4.50	4.59	3.86	3.45
22	6.14	6.39	6.87	6.62
23	6.65	6.95	7.45	7.15
25	2.35	2.22	2.21	2.27
26	3.17	3.13	3.21	3.33
29	3.08	3.03	2.92	3.52

[a] Reference 18. [b] Reference 17.

tives showed the highest affinity. For the nonpolar hydantoins (i.e., **7**, **12**, **15**, **17**, and **22**), CB$_1$ affinity decreased in the following order Br > OMe > F > Me > H, whereas such a relationship was not observed for the polar hydantoins (i.e., **11**, **14**, **16**, **20**).

On the basis of these results, various modifications were carried out at position N$_3$ of the hydantoin moiety (Table 1). It turned out that whatever the nature of the R$_1$ substituent, CB$_1$ affinity increased with increasing length of the alkyl group and hence with lipophilicity. For example, compound **8** showed a higher CB$_1$ affinity than compound **4**. However, the case of compounds **20**−**23** is not straightforward. Compounds **20**−**21** have a remarkably low log P_{calc} value in contrast with compound **23** (Table 4), yet their CB$_1$ affinity was higher (Table 1). This would suggest that lipophilicity of the side chain at position N$_3$ alone does not explain variations in CB$_1$ affinity, and that the CB$_1$ receptor can also accommodate ligands having a polar moiety (hydroxy or morpholino group) on this chain, as demonstrated by compounds **20**−**21**. Finally, no displacement of the radioligand at 10 μM was observed with compounds **2** and **3**, suggesting that the introduction of a basic amino group on the alkyl side chain is unfavorable to CB$_1$ binding.

X-ray Analysis. Two independent molecules (mol100 and mol200) are found in the asymmetric unit of the crystal structure of compound **20**. They form a dimer connected by a H-bond between N$_5$ and O$_1$ (O···N distance about 3.2 Å, see Table 5), suggesting that these groups could form intermolecular interactions with the CB$_1$ receptor. An ORTEP diagram of the two molecules in the asymmetric unit of the crystal cell is presented in Figure 3, and selected geometries are given in Table 5. As expected, the hydantoin rings are planar, with the N and C atoms adopting an sp^2 hybridization. Bond lengths within the ring are intermediate between single and double bonds, implying electronic delocalization in the system.

The perpendicular orientation of the two bromophenyl rings is similar in both molecules, allowing optimal $\pi-\pi$ and quadrupole interactions in the crystal packing. The morpholino ring adopts a stable chair conformation in both independent molecules (mol100 and mol200) while the conformation adopted by the lateral ethylmorpholino group differs in both molecules (see τ1, τ2, τ3 in Table 5).

Binding Mode Hypothesis and Molecular Field Calculation. The previous synthesis of HHC and

Table 5. Selected Geometries of the X-ray Structure of Compound **20**

	mol 100	mol 200
	Bond Lengths (Å)	
O1−C2	1.215(3)	1.219(3)
C2−N3	1.352(2)	1.352(2)
N3−C4	1.402(2)	1.407(3)
C4−N5	1.347(3)	1.344(3)
N5−C6	1.460(3)	1.458(3)
C6−C2	1.547(3)	1.546(3)
C4−O7	1.213(3)	1.212(3)
	Bond Angles (deg)	
O1−C2−N3	126.7(4)	127.0(4)
C2−N3−C4	112.0(4)	111.8(3)
N3−C4−N5	107.4(3)	107.3(4)
C4−N5−C6	112.7(4)	112.7(4)
N5−C6−C2	100.6(3)	100.5(4)
C6−C2−N3	107.0(4)	107.0(4)
N3−C4−O7	124.4(4)	123.8(4)
	Torsion Angles (deg)	
$\tau 1$	69.9(5)	102.8(4)
$\tau 2$	58.7(5)	−60.5(5)
$\tau 3$	−161.5(4)	−75.5(5)
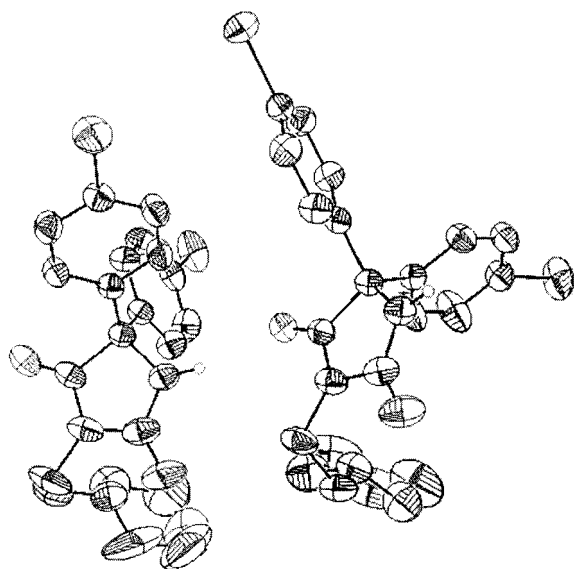
Figure 3. ORTEP diagram (50% probability) obtained from the X-ray structure of **20** showing the association of the two molecules in the asymmetric unit.

extensive SAR studies[2] have yielded useful information on the structural requirements of cannabinoid affinity, namely (1) a hydrophobic C_3 alkyl side chain (SC), (2) a phenolic group (PH), and (3) the northern aliphatic hydroxy group (NAH) (Figure 4). Furthermore, experimental evidence has indicated that the pyran oxygen is not part of this model and can be replaced by a carbon or nitrogen atom, or removed ring with opening, without extensive loss of potency[2] (see CP-47,497 and CP-55,-940).

Molecular lipophilic potential (MLP)[18] and molecular hydrogen bonding potentials[23] studies have allowed us here to establish the elements by which hydantoin
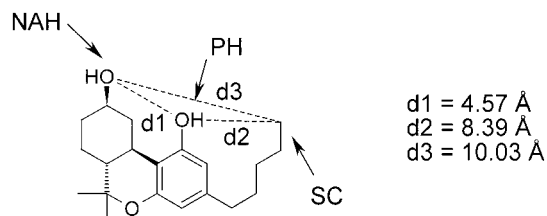
Figure 4. Distances measured on the three-point HHC pharmacophore, namely SC, the hydrophobic alkyls side chain; PH, the phenolic group, and NAH, the northern aliphatic hydroxy group.
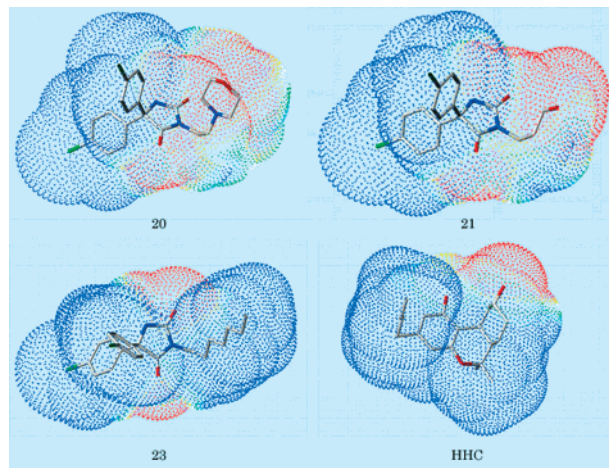
Figure 5. Molecular lipophilic potential of **20**, **21**, **23**, and HHC. The polar regions are represented in red and the nonpolar in blue.

derivatives could interact with the CB_1 receptor. The preferred conformation of the analogues were defined using the solid-state structures of compound **20** (mol100) (Figure 3). The torsion angles $\tau 1$, $\tau 2$, and $\tau 3$ (Table 5) were adjusted by hand on the templates defined by the solid-state structures of compound **20** (mol100, Table 5) to obtain consistent conformations through the series, and the structures were energy-minimized by molecular mechanics calculations. The MLP generated by these analogues was then calculated using the CLIP program.[18] The results confirm the known differences in log P values between the polar hydantoins (i.e., having a morpholino or hydroxy group on the alkyl side chain) and their nonpolar analogues. As depicted in Figure 5, two important hydrophobic regions separated by a small polar region exist in nonpolar hydantoins, whereas only one polar and one hydrophobic region are generated around the polar hydantoins (**11**, **15**, **16**, **20**, **21**). For both families of hydantoins (i.e., polar and nonpolar), an important hydrophobic region is generated around the phenyl rings. The MLP generated around HHC (Figure 5) was also calculated and is characterized by one important hydrophobic region (blue), located on the hydrophobic C_3 alkyl side chain (Figure 5), and one small polar region (red) located near the phenolic and northern aliphatic hydroxy groups (Figure 5). Examination of the MLPs suggests that HHC and hydantoins could be stabilized within the active site of the CB_1 receptor by their hydrophobic C_3 alkyl side chain or phenyl rings, respectively.

A new computational tool known as the molecular hydrogen bonding potentials[23] (MHBPs) was also used to identify the groups potentially able to contribute to
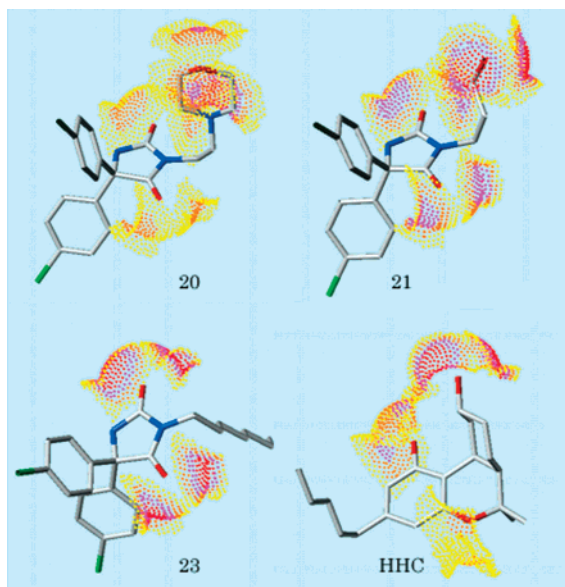
Figure 6. Molecular hydrogen bonding potential of **20**, **21**, **23** and HHC. Red, magenta, and yellow iso-potential contours correspond to three levels of values (acceptor MHBPs: 0.15, 0.10, and 0.05).

the binding by H-bond formation. The MHBPs involve the same stepwise procedure as used previously to generate the MLP. First, a H bonding fragmental system (Systahl version 1.0) derived from literature donor (α) and acceptor (β) values identifies the structural elements (polar hydrogen atoms and lone pairs) able to form H-bonds and assigns a fragmental value to each of them. The MHBPs are then calculated for each point k on a molecular surface or in a 3D-grid according to eq 1

$$\text{MHBP}_k = \sum_{i=1}^{N_{\text{frg}}} \sum_{j=1}^{n_{\text{at}}} F_{ij}\, f(d_{jk})\, g(U_{jk}) \qquad (1)$$

where k is the label of the point in space, N_{frg} the number of molecular fragments in the compound, n_{at} the number of polar atoms in the molecular fragment i, F_{ij} the α and/or β value of atom j in the fragment i, d_{jk} the distance between the polar atom j and the point k, $f(d_{jk})$ the distance function, U_{jk} the angle defined by the point k, the polar atom j, and the polar hydrogen or the lone pair belonging to the polar atom j, and $g(U_{jk})$ the angular function.[23] This new computational tool was compared with GRID interactions energies[24] and has been used successfully in structure−absorption relations.[23]

For both families of hydantoins (i.e., polar and nonpolar), two H bond-accepting potentials appear around the carbonyls (Figure 6). A third hydrogen accepting potential is also generated by the morpholino and hydroxy groups present in polar hydantoins (Figure 6). The analysis of HHC shows that H-bond accepting potentials are generated around the phenolic group, the northern aliphatic hydroxyl, and the oxygen heteroatom of the furan ring (Figure 6).

Molecular Superposition. Examination of the MHBPs and MLP of hydantoins and HHC (Figures 5 and 6) shows that the three pharmacophoric groups in HHC (Figure 7) match the corresponding groups in the polar
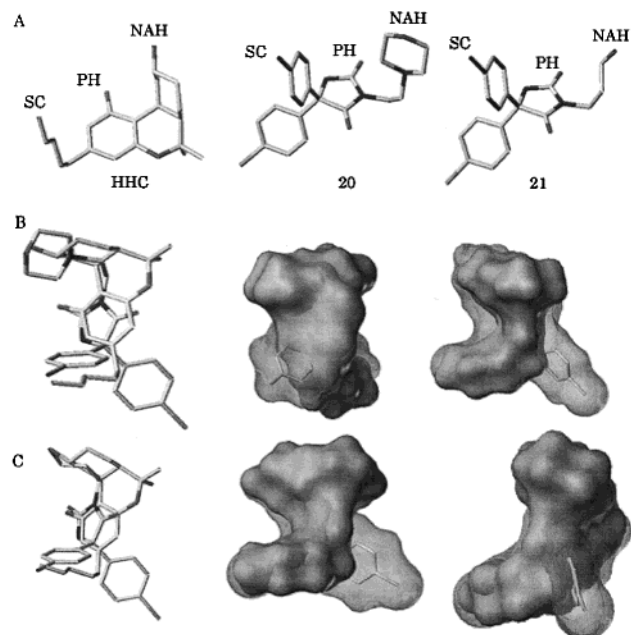

Figure 7. (A) Groups (i.e., SC, PH, NAH) used for the superposition of compounds **20**−**21** and HHC. (B) Alignment obtained from the RMS fitting between HHC and **20**, and orthogonal views of the Connoly surfaces calculated on **20** (gray) and HHC (dark gray). (C) Alignment obtained from the RMS fitting between HHC and **21**, and orthogonal views of the Connoly surfaces calculated on **21** (gray) and HHC (dark gray).

hydantoins, namely (1) the oxygen atom of the morpholino or hydroxy moiety, (2) the oxygen atom of the carboxyl amide, and (3) the phenyl rings (Figure 7). On the basis of these similarities, structural alignment between the polar hydantoins and HHC was achieved by root-mean-square (rms) fitting. As depicted in Figure 8, the polar hydantoins and HHC, although structurally different, can optimally be aligned. The Connoly surface generated by the compounds were then calculated using this superposition. In this view, one can see that the overall shape of HHC is closely mimicked by the superposed hydantoins. It appears that the Connoly surfaces of the morpholino group is confined to a region that would be predicted to permit pharmacological activity (i.e., there does not appear to be hydantoins volume at the C_9−C_{11} position that has previously been associated with decreased cannabinoid potency). Furthermore, it appears that *pro-R* phenyl ring fits well with the alkyl side chain of HHC, whereas *pro-S* phenyl ring generates steric hindrance. This suggests that the CB_1 affinity of our compounds could be improved by a more appropriate subsition of the C_1 position of the hydantoin. However, the *pro-S* phenyl ring could also be responsible of the pure antagonist profile of compounds **20**, **21**, and **23**. Indeed, according to Ariën's theory, the modulation of the agonist to antagonist activity can be obtained through the addition of some supplementary aromatic rings that play the role of additional binding sites (e.g., the passage from muscarinic agonists to muscarinic antagonists or from GABA agonists to GABA antagonists[25]).

Alignment was also investigated for HHC and the nonpolar hydantoins, using two pairs of atoms (i.e., the hydantoin carbonyls and the oxygen atoms in rings A and B of HHC), revealing two distinct superimpositions
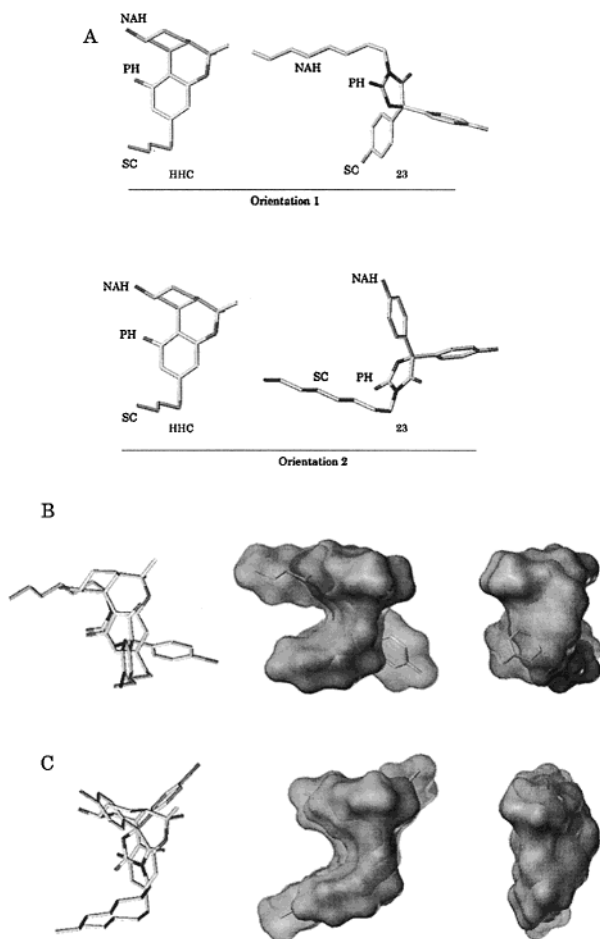
Figure 8. (A) Groups (i.e., SC, PH, NAH) used for the superposition of compounds **23** and HHC. (B) (orientation 1) Alignment obtained from the RMS fitting between HHC and **23**, and orthogonal views of the Connoly surfaces calculated on **23** (gray) and HHC (dark gray). (C) (orientation 2) Alignment obtained from the RMS fitting between HHC and **23**, and orthogonal views of the Connoly surfaces calculated on **23** (gray) and HHC (dark gray).

(Figure 8). These results can be explained as in Figure 5 by the fact that the MLP generated around the nonpolar hydantoins is characterized by two important hydrophobic regions separated by a small polar one. As shown by the Connoly surfaces (Figure 8), the best alignment corresponds to orientation 2. Indeed, the two phenyl rings in the hydantoins are well aligned with HHC rings, and the alkyl side chains are optimally aligned. Such a close alignment was not obtained with orientation 1, since the alkyl side chain of **23** does not fit well with the northern aliphatic hydroxy of HHC and the *pro-R* phenyl ring generates steric hindrance (Figure 8). Although HHC is an agonist and hydantoins are antagonists, several authors[26−28] suggest a common pharmacopohore for cannabinoid ligands whatever the full, partial, or inverse agonist properties of the ligand. In the absence of site directed mutagenesis data giving a clue about the amino acids involved in the hydantoin recognition on one hand and of a 3-D structure of the CB$_1$ receptor on the other hand, the superimposition of hydantoins to HHC was made in a first intention.

These results suggest that the polar hydantoins adopt a binding mode (orientation 1) different from that of nonpolar hydantoins (orientation 2). This dual binding mode is consistent with the fact that the presence of a hydroxy on the C$_9$ position of HHC is not essential for affinity.[2] It is also in agreement with the SAR results, since CB$_1$ affinity of nonpolar hydantoins decreases in the order Br > MeO > F $\cong$ Me > H, whereas for polar hydantoins such ranking was not observed. Further ligands bearing only one aromatic ring in position 5 are under study to confirm this model and improve the affinity while retaining antagonism.

Conclusion

The comparison of the molecular lipophilic potential and the molecular hydrogen bond potential generated around hydantoins and HHC has led to a superimposition model for this new class of CB$_1$ ligands and probable antagonists. This model suggests that there are key elements common to HHC and hydantoins and that these compounds are stabilized within the active site of the CB1 receptor through hydrophobic and H-bond interactions. The superimposition model also addresses the unfavorable steric interaction generated by the substituents on the hydantoin ring. Rational synthesis of further ligand is under progress to enhance the CB$_1$ affinity of this new class of compounds and to confirm this three-point CB$_1$ binding mode hypothesis.

Compounds **20**, **21**, and **23** represent the first neutral antagonists of the cannabinoid receptors. Regarding the originality of structure and of mechanism of action, they may constitute new pharmacological tools as well as potential therapeutic agents in the control of appetite, learning, and memory.

Experimental Section

Chemistry. Melting points were determined on a Büchi SMP 20 capillary instrument and are uncorrected. The purity of the compounds was checked by TLC on aluminum-covered plates of siliga gel Merck 60F$_{254}$ and by RP-HPLC (Perkin-Elmer 100-LC with LC-85B UV detector set at 254 nm and Integrator LCI-100) using a C18 HL 90−5S Bio-Rad column (250 mm, internal diameter 4.6 mm, particles size 5 μM), a mobile phase consisting of methanol and phosphate buffer pH 7.4, and a flow rate of 1 mL/min. Infrared spectra were recorded as KBr pellets using a Perkin-Elmer 297 spectrometer. Absorption values are expressed as wavenumbers (cm^{-1}). Elemental analyses were performed on a Carlo Erba EA 1108 Analyzer (Carlo-Erba, Milano, Italy) and are within ±0.4% of the theoretical values. ^{13}C NMR were recorded at ambient temperature on a AC-300 Bruker spectrometer. The chemical shifts are reported as δ (ppm) values relative to tetramethylsilane. Mass spectra were recorded on a Varian MAT 44 S (E.I. 70 eV, source 200 °C), with the kind help of Prof. G. Scriba (Iena University, Germany). Optical rotations were measured using a Perkin-Elmer 241 MC polarimeter operating at 589 nm and room temperature.

Preparation of 3-Alkyl-(5,5′-diphenyl)imidazolidinediones (1−24). The *N*-3-substituted(5,5′-diphenyl)hydantoins **1−24** were synthesized as described elsewhere.[16]

Preparation of 3-Alky-5-(indo-3-yl)imidazolidinediones (25−29). To a solution of 0.01 mol of the 5-(indol-3-yl-methyl)imidazolidinedione (prepared as previously described)[29] in DMF in the presence of 0.04 mol of potassium carbonate was added 0.012 mol of the respective alkyl chloride, and the solution was stirred overnight at room temperature. The product was obtained after addition of water, and the precipitate was recrystallized from ethanol. 5-(Indol-3-yl-methyl)-imidazolidinedione was prepared from tryptophane (0.146 mol) and potassium isocyanate (0.493 mol) in 200 mL water. The mixture was stirred and heated at 80 °C for 30 min. After cooling, 70 mL of 6 M HCl was added to precipitate the hydantoic acid. The latter gave the desired cyclic compound

after heating for 2 h at reflux temperature in a mixture of 1 L of 3 M HCl and 0.2 L of ethanol. The resulting precipitate was recrystallized in propan-2-ol.

5-(Indol-3-yl-methyl)imidazolidinedione: yield 77%; mp 249−251 °C (uncorrected); mass spectrometry [M$^\bullet$] = 238, [M$^{\bullet+1}$] = 239; ^{13}C NMR δ (DMSO-d_6) 26.76(CH$_2$), 58.55(CH), 108.23, 111.46, 118.56, 118.82, 121.07, 124.35, 127.74, 136.15-(C and CH arom.), 157.64(C=O), 175.98(C=O).

(±)-3-Butyl-5-(indo-3-yl)imidazolidinedione (25): yield 65%; mp 142−144 °C (uncorrected); mass spectrometry [M$^\bullet$] = 285, [M$^{\bullet+1}$] = 286; ^{1}H NMR δ (DMSO-d_6) 0.76(t,3H), 1.01-(m,4H), 3.10(d,2H), 3.40(t,2H), 4.32(d, 1H), 7.11−8.16(m, 5H), 10.88(s, 1H); ^{13}C NMR δ (DMSO-d_6) 13.32(CH$_3$), 18.84(CH$_2$), 26.51(CH$_2$), 29.19(CH$_2$), 36.92(CH$_2$), 56,82(CH), 107.41, 111.08, 118.19, 118.57, 120.71, 124.22, 127.40, 135.88(C and CH arom.), 156.86(C=O), 173.94(C=O). Anal. (C$_{16}$H$_{19}$N$_3$O$_2$) C, H, N.

(±)-3-Hexyl-5-(indo-3-yl)imidazolidinedione (26): yield 61%; mp 135−137 °C (uncorrected); mass spectrometry [M$^\bullet$] = 313, [M$^{\bullet+1}$] = 314; ^{1}H NMR δ (DMSO-d_6) 0.82(t,3H), 1.21-(m,8H), 3.05(d,2H), 3.55(t,2H), 4.33(d, 1H), 6.93−7.79(m,d,d, 5H), 10.85(s, 1H); ^{13}C NMR δ (DMSO-d_6) 12.92(CH$_3$), 20.16-(CH$_2$), 23.76(CH$_2$), 24.94(CH$_2$) 25.41(CH$_2$), 29.02(CH$_2$), 35,62-(CH$_2$), 55.95(CH), 105.79, 109.47, 116.56, 116.95, 119.08, 122.63, 125.79, 134.26(C arom.), 155.24(C=O), 172.35(C=O). Anal. (C$_{18}$H$_{23}$N$_3$O$_2$), C, H, N.

(±)-3-Ethylphenyl-5-(indo-3-yl)imidazolidinedione (27): yield 79%; mp 159−161 °C (uncorrected); mass spectrometry [M$^\bullet$] = 333; ^{1}H NMR (CDCl$_3$) 3.19(d,1H), 4.07(s,1H), 4.57(d,-1H), 6.95−7.98(m, 10H); ^{13}C NMR (CDCl$_3$) 24.40(CH$_3$), 42.36-(CH$_2$), 44.88(CH$_2$), 58.86(CH), 108.06, 111.23, 118.56, 119.79, 122.21, 123.06, 127.34,127.44, 128.02, 128.23, 135.57, 135.83-(C arom), 156.70(C=O), 172.57(C=O). Anal. (C$_{20}$H$_{19}$N$_3$O$_2$) C, H, N.

(±)3-Propylphenyl-5-(indo-3-yl)imidazolidinedione (28): yield 75%; mp 153−155 °C (uncorrected); mass spectrometry [M$^\bullet$] = 347, [M$^{\bullet+1}$] = 348; ^{1}H NMR (CDCl$_3$) 1.76(q,2H), 2.48-(t,2H), 3.03(d,2H), 3.40(t,2H), 4.21(d, 1H), 7.01−8.03(m,d,d,s, 5H), 10.76(s, 1H); ^{13}C NMR (CDCl$_3$) 27.80(CH$_2$), 29.09(CH$_2$), 32.82(CH$_2$), 38.36(CH$_2$), 57.75(CH$_2$), 109.32, 111.33, 118.62, 119.87, 122.43, 123.15, 125.99, 127.04, 128.29, 128.37, 136.18, 141.09(C and CH arom.), 157.55(C=O), 173.66(C=O). Anal. (C$_{21}$H$_{21}$N$_3$O$_2$) C, H, N.

(±)-3-(1-Naphthylmethyl)-5-(indo-3-yl) imidazolidinedione (29): yield 56%; mp 176−178 °C (uncorrected); mass spectrometry [M$^\bullet$] = 369, [M$^{\bullet+}$] = 370; ^{1}H NMR (DMSO-d_6) 3.06(d,2H), 3.97(s,2H), 4.29(d,1H), 6.41−8.41(m,12H), 10.91-(s,1H); ^{13}C NMR (DMSO-d_6) 26.44(CH$_2$), 40.52(CH$_2$), 57.76-(CH$_2$), 107.8, 111.49, 118.69, 119.03, 121.14, 123.15, 124.76, 127.28, 136.17(C and CH arom)$_{indol.}$, 122.92, 125.42, 125.94, 126.40, 126.81, 127.83, 128.60, 130.16, 131.23, 133.14 (C and CH arom.)$_{napht.}$, 156.74(C=O), 174.13(C=O). Anal. (C$_{23}$H$_{19}$N$_3$O$_2$) C, H, N.

Pharmacology. Fatty acid free bovine serum albumin (fafBSA) was purchased from Sigma Chemical Co (St. Louis, MO). WIN-55,212-2 was purchased from RBI (Natick, MA), HU-210, and CP-55,940 from Tocris (Bristol, U.K.). SR-141716A was kindly donated by Sanofi Recherche (Montpellier, France). [^{3}H]-SR-141716A (1.92 TBq/mmol, 52 Ci/mmol) was from Amersham (Roosendaal, The Netherlands).

1. Inhibition of [^{3}H]-SR-141716A Binding in CB$_1$-Transfected CHO Cells. CB$_1$-transfected CHO cells,[5] kindly donated by Prof. Vassart (Université Libre de Bruxelles) and Dr. Nokin (Euroscreen, Brussels), were maintained in culture using Ham F12 medium (Gibco BRL) containing 10% fetal calf serum, 100 μg/mL streptomycin, 100 U/mL penicillin, and 200 μg/mL G418 (Gibco BRL). Membranes (60 μg) obtained from transfected CHO cells expressing human CB$_1$ cannabinoid receptors were incubated in siliconized plastic tubes at 30 °C with 1 nM [^{3}H]-SR-141716A for 1 h in 50 mM Tris-HCl (pH 7.4) with 3 mM MgCl$_2$, 1 mM disodium EDTA, and 0.1% bovine serum albumin (BSA). Nonspecific binding was determined with 10 μM WIN-55,212−2 or 10 μM CP-55,940. Finally, the membrane was rapidly filtered on 0.5% polyethylemeneimine

(PEI) pretreated GF/C glass fiber filters (Whatman) and washed twice with 5 mL of ice-cold incubating buffer without serum albumin. Radioactivity on filters was measured with a Pharmacia Wallac 1410 β-counter by liquid scintillation in 10 mL of Aqualuma. Assays were performed in triplicates.

2. Binding of [^{35}S]GTPγS in Rat Cerebella Membranes. The binding experiment was performed at 30 °C in plastic tubes containing 20 μg of protein resuspended in 1 mL (final volume) of binding buffer (50 mM Tris-HCl (pH 7.4), 5 mM MgCl$_2$, 1 mM disodium EDTA, 100 mM NaCl, 0.1% (w/v) bovine serum albumin) supplemented with 20 μM GDP and 0.01 nM−100 μM agonist or antagonist. The binding was initiated by the addition of [^{35}S]-GTPγS (0.05 nM final concentration). Incubations were performed for 1 h and were terminated by addition of 3 mL of ice-cold washing buffer (50 mM Tris-HCl, pH 7.4; 5 mM MgCl$_2$; 1 mM disodium EDTA; 100 mM NaCl). The suspension was immediately filtered through GF/B filters using a 24-well Brandel cell harvester and washed twice with ice-cold binding buffer. Radioactivity trapped on the filters was counted as mentioned above. The nonspecific binding was measured in the presence of 0.1 mM Gpp(NH)p.

Data Analysis. Radioligand and nucleotide binding data were analyzed by nonlinear regression with the software GraphPad Prism, version 3.00 (GraphPad, San Diego, CA). Antagonist equilibrium dissociation constants (expressed as pK_B) were calculated using the following equation

$$K_B = A/(CR - 1)$$

where A is the concentration of antagonist used and CR is the ratio of EC$_{50}$ values for the agonist measured in the presence or in the absence of the antagonist, respectively.

Structural, Physicochemical, and Computational Investigations. 1. Crystal Structure. Single crystals of compound **20** were obtained by slow evaporation of concentrated solutions in ethanol. A suitable crystal was mounted on a quartz fiber on a goniometer head of a CAD4 Nonius diffractometer. After determination of the cell parameter using 25 well-centered reflections, complete diffraction data sets were collected. The structure was solved using direct methods and refined by full matrix least squares on F^2 using the program Shelxl97.[30] All non-hydrogen atoms were treated anisotropically while a riding model was applied for the hydrogens. Analytical correction for absorption was introduced.

Compound **20**: triclinic, P-1, a = 12.382(2) Å, b = 12.718(2) Å, c = 14.438(2) Å, α = 112.31 (1)°, β = 92.73 (1)°, γ = 92.30-(1)°, V = 2096.1 (2) Å^3, Z = 2 (two molecules in the asymmetric unit), μ = 5.14 mm^{-1}, D_x = 1.627 g cm^{-3}, λ (Cu Kα) = 1.54178 Å, F(000) = 1048, T = 290 K, 8229 unique reflections (R_{int} = 0.0166), R_1 = 0.0444 for 7500 F_o > 4σ(F_o), R_1 = 0.0483 for all data (8229) and wR_2 = 0.1356, GOF = S = 1.075.

2. Molecular Models and Calculation of Molecular Interaction Fields. All calculations were performed on Silicon Graphics Indy R4400 175 MHz, O$_2$ R5000 180 MHz, or Origin 2000 4·R10000 195 MHz workstations using the SYBYL 6.5 molecular modeling package (Tripos Associates, St. Louis, MO) including SLN (Sybyl line notation) and CONCORD (connectivity to coordinates) algorithm.[31]

The starting geometries of the hydantoins and HHC were built by CONCORD. The C$_3$ alkyl side chain of HHC was oriented perpendicularly to the aromatic ring by adjusting both the τ_1 and τ_2 torsion angles to 60° and 120°, respectively. These values correspond to one of the four low-energy conformations previously identified by Xie et al.[32] The torsion angles τ_1, τ_2, and τ_3 of hydantoins were adjusted using the solid-state structure of compound **20** (mol1 100, see Table 5). Each structure was then energy-optimized using the MMFF94s force field including MMFF94 partial atomic.[33,34] As a test, the geometry of compound **20** was first optimized and proved in good agreement with the experimental crystal structures.

The molecular lipophilic potential[18] and molecular hydrogen bonding potentials[23] were calculated on the solvent accessible surface area.

3. Experimental Lipophilicity Determination by RP-HPLC. Because the log P value of the investigated compounds could not be determined by the traditional shake-flask method, lipophilicity indices were measured by a reversed-phase HPLC method (RP-HPLC) consisting in a Perkin-Elmer Series 10 LC apparatus linked to a Perkin-Elmer LCI-100 integrator and a UV Perkin-Elmer detector set at 250 nm. The capacity factors were measured with a Bio RAD Bio Sil C18 HL 90-5S column (length 250 mm, internal diameter 4.6 mm, and particles size 5 μM) with four different mobile phases (methanol/phosphate buffer 0.1 M pH 7.4 ratios = 90:10, 80:20, 75:25, and 70:30 v/v). The capacity factor (k') was defined for each mixture as the $(t_r - t_0)/t_0$ where t_r is the retention time of the solute, and t_0 the column dead time. The log k_w corresponding to the logarithm of the apparent capacity factor for a concentration of methanol of 0% was then obtained by linear extrapolation of experimental log k' values.[35-36]

4. Calculation of log P Values. Two different procedures were used to calculate the log P of the hydantoin derivatives (Tables 1–3), namely the CLOGP algorithm[17] and the MLP using the CLIP program.[18] In the MLP calculations, the input geometry of compound **20** was that of its X-ray structure, whereas the structure of the other compounds was optimized by molecular mechanics.

Supporting Information Available: Crystallographic parameters for the structure of compound **20**. This material is available free of charge via the Internet at http://pubs.acs.org.

References

(1) Gaoni, Y.; Mechoulam, R. Isolation, structure and partial synthesis of an active constituent of hashih. *J. Am. Chem. Soc.* **1964**, *86*, 1645–1646.

(2) Khanolkar, D. A.; Palmer, S. L.; Makriyannis, A. Molecular probes for the cannabinoid receptors. *Chem. Phys. Lipids* **2000**, *108*, 37–52.

(3) Devane, W. A.; Dysarz, F. A.; Johnson, M. R.; Melvin, L. S., Howlett, A. C. Determination and characterization of a cannabinoid receptor in rat brain. *Mol. Pharmacol.* **1988**, *34*, 605–613.

(4) Matsuda, L. A.; Lolait, S. J.; Brownstein, M. J.; Young, A. C.; Bonner, T. I. Structure of a cannabinoid receptor and functional expression of the cloned cDNA. *Nature* **1990**, *346*, 561–564.

(5) Gérard, C. M.; Mollereau, C.; Vassart, G.; Parmentier, M. Molecular cloning of a human cannabinoid receptor which is also expressed in testis. *Biochem. J.* **1991**, *279*, 129–134.

(6) Shire, D.; Carillon, C.; Kaghad, M.; Calandra, B.; Rinaldi-Carmona, M.; Le Fur, G.; Caput, D.; Ferrara, P. An amino-terminal variant of the central cannabinoid receptor resulting from alternative splicing. *J. Biol. Chem.* **1995**, *270*, 3726–3731.

(7) Munro, S.; Thomas, K. L.; Abu-Shaar, M. Molecular characterization of a peripheral receptor for cannabinoids. *Nature* **1993**, *365*, 61–65.

(8) Shire, D.; Calandra, B.; Rinaldi-Carmona, M.; Oustric, D.; Pessegue, B.; Bonnin-Cabanne, O.; Le Fur, G.; Caput, D.; Ferrara, P. Molecular cloning, expression and function of the murine CB2 peripheral cannabinoid receptor. *Biochim. Biophys. Acta* **1996**, *1307*, 132–136.

(9) Griffin, G.; Tao, Q.; Abood, M. E. Cloning and pharmacological characterization of the rat CB2 cannabinoid receptor. *J. Pharmacol. Exp. Ther.* **2000**, *292*, 886–894.

(10) Howlett, A. C. Cannabinoid inhibition of adenylate cyclase: relative activity of constituents and metabolites of marihuana. *Neuropharmacology* **1987**, *26*, 507–512.

(11) Mackie, K.; Hille, B. Cannabinoids inhibit N-type calcium channels in neuroblastoma-glioma cells. *Proc. Natl. Acad. Sci. U.S.A.* **1992**, *89*, 3825–3829.

(12) Gebremedhin, D.; Lange, A. R.; Campbell, W. B.; Hillard, C. J.; Harder, D. R. Cannabinoid CB1 receptor of cat cerebral arterial muscle functions toinhibit L-type Ca²⁺ channel current. *Am. J. Physiol.* **1999**, *276*, H2085–2093.

(13) Deadwyler, S. A.; Hampson, R. E.; Mu, J.; Whyte, A.; Childers, S. Cannabinoids modulate voltage sensitive potassium A-current in hippocampal neurons via a cAMP-dependent process. *J. Pharmacol. Exp. Ther.* **1995**, *273*, 734–743.

(14) Bouaboula, M.; Poinot-Chazel, C.; Bourrie, B.; Canat, X.; Calandra, B.; Rinaldi-Carmona, M.; Le Fur, G.; Casellas, P. Activation of mitogen-activated protein kinases by stimulation of the central cannabinoid receptor CB1. *Biochem J.* **1995**, *312*, 637–641.

(15) Di Marzo, V.; Bisogno, T.; De Petrocellis, L.; Melck, D.; Martin, B. R. Cannabimimetic fatty acid derivatives: the anandamide family and other endocannabinoids. *Curr. Med. Chem.* **1999**, *6*, 7 21–744.

(16) Kanyonyo, M. R.; Govaerts, S. J.; Hermans, E.; Poupaert, J. H.; Lambert, D. M. 3-Alkyl-(5,5'-diphenyl)imidazolidinediones as new cannabinoid receptor ligands. *Bioorg. Med. Chem. Lett.* **1999**, *9*, 2233–2236.

(17) DAYLIGHT software 4.41, 1995, Daylight Chemical Information System, Inc., Irvine, CA.

(18) Gaillard, P.; Carrupt, P. A.; Testa, B. and Boudon, A. Molecular lipophilicity potential, a tool in 3D-QSAR. Method and applications. *J. Comput.-Aided Mol. Des.* **1994**, *8*, 83–96.

(19) Sim, L. J.; Selley, D. E.; Childers, S. R. In vitro autoradiography of receptor-activated G proteins in rat brain by agonist-stimulated guanylyl5'-[gamma-[35S]thio]-triphosphate binding. *Proc. Natl. Acad. Sci. U.S.A.* **1995**, *92*, 7242–7246.

(20) Kearn, C. S.; Greenberg, M. J.; Dicamelli, R.; Kurzawa, K.; Hillard, C. J. Relationships between ligand affinities for the cerebellar cannabinoid receptor CB1 and the induction of GDP/GTP exchange. *J Neurochem.* **1999**, *72*, 2379–2387.

(21) Pertwee, R. G. Pharmacology of cannabinoid receptor ligands. *Curr. Med. Chem.* **1999**, *6*, 635–664.

(22) Suzuki, T.; Kudo, Y. Automatic logP estimation based on combined additive modeling methods. *J. Comput.-Aided Mol. Des.* **1990**, *4*, 155–198.

(23) Rey, S. Caron, G.; Ermondi, G.; Gaillard, P.; Pagliara, A.; Carrupt, P.-A.; Testa, B. Development of molecular hydrogen-bonding potentials (MHBPs) and their application to structure-permeation relations *J. Mol. Graphics* **2001**, *19*, 521–535.

(24) Boobbyer, D. N. A.; Goodford, P. J.; McWhinnie, P. M.; Wade, R. C. New hydrogen-bond potentials for use in determining energetically favorable binding sites on molecules of known structure. *J. Med. Chem.* **1989**, *32*, 1083–1094.

(25) Wermuth, C. G. Strategies in the search for new lead compounds or original working hypotheses. In *The Practice of Medicinal Chemistry*, 1st ed.; Wermuth, C. G., Eds; Academic Press: London, 1996; pp 81–99.

(26) Fichera, M.; Cruciani, G.; Bianchi, A.; Musumarra, G. A 3D-QSAR study on the structural requirements for binding to CB-(1) and CB(2) structural receptors. *J. Med. Chem.* **2000**, *43*, 2300–2309.

(27) Reggio, P. H. Ligand-ligand and ligand–receptor approaches to modeling the cannabinoid CB1 and CB2 receptors: achievements and challenges. *Curr. Med. Chem.* **1999**, *6*, 665–683.

(28) Thomas, B. F.; Adams, I. B.; Mascarella, S. W.; Martin, B. R.; Razdan, R. K. Structure–activity analysis of anandamide analogues: relationship to a cannabinoid pharmacophore. *J. Med. Chem.* **1996**, *39*, 471–479.

(29) Boyd, W. J. The isolation of amino acids in the form of the corresponding carbamido-acids and hydantoins. *Biochem. J.* **1933**, *27*, 1833–1843.

(30) Sheldrick, G. *Shelxl97*, Program for the refinement of molecular crystal structures, 1997, University of Göttingen, Germany.

(31) Pearlman, R. S.; Balducci, R.; Rusinko, A.; Skell, J. M.; Smith, K. M. 1993, Tripos Associates, Inc., St. Louis, MO.

(32) Xie, X. Q.; Yang, D. P.; Melvin, L. S.; Makriyannis, A. Conformational analysis of the prototype nonclassical cannabinoid CP-47,497, using 2D NMR and computer molecular modeling. *J. Med. Chem.* **1994**, *37*, 1418–1426.

(33) Halgren, T. A. MMFF VII. Characterization of MMFF94, MMFF94s, and other widely available force fields for conformational energies and for intermolecular interaction energies and geometries. *J. Comput. Chem.* **1999**, *20*, 730–748.

(34) Halgren, T. A. MMFF VI. MMFF94s option for energy minimization studies. *J. Comput. Chem.* **1999**, *20*, 720–729.

(35) Bechalany, A.; Röthlisberger, T.; El Tayar, N; Testa, B. Comparison of various nonpolar stationary phases used for assessing lipophilicity. *J. Chromatogr.* **1989**, *473*, 115–124.

(36) Altomare, C.; Tsai, R. S.; El Tayar, N.; Testa, B.; Carotti, A.; Cellamare, S.; De Benedetti, P. G. Determination of lipophilicity and hydrogen-bond donor acidity of bioactive sulphonyl-containing compounds by reversed-phase HPLC and centrifugal partition chromatography and their application to structure–activity relations. *J. Pharm. Pharmacol.* **1991**, *43*, 191–197.